Iranian Journal of Catalysis 8(2), 2018, 113-120

IRANIAN JOURNAL OF CATALYSIS

Incorporation of Pb^{2+}, Fe^{2+} and Cd^{2+} ions in ZnO nanocatalyst for photocatalytic activity

Maryam Bordbar[a,*], Zahra Sayban[b], Ali Yeganeh-Faal[b], Bahar Khodadadi[a]

[a]*Department of Chemistry, Faculty of Science, University of Qom, Qom, Iran.*

[b]*Faculty of Science, Payame Noor University, Qom, Iran.*

Received 6 October 2017; received in revised form 29 December 2017; accepted 29 January 2018

ABSTRACT

In the present study, Pb-ZnO, Fe-ZnO, Cd-ZnO and Pb-Fe-Cd-ZnO nanoparticles were synthesized by the sonochemical method and those structural and optical properties were investigated by Fourier Transform Infrared spectroscopy (FTIR), UV-Vis spectroscopy, Field Emission Scanning Electron Microscopy (FE-SEM) and X-Ray Diffraction (XRD). Average crystallite size obtained was 60 nm. Moreover, the direct band gap has been calculated using Tauc's approach. Compared with pure ZnO, the band gap of the doped-ZnO NPs is smaller and it depends on the type of dopants. In addition, photocatalytic activity of all samples has been investigated by the degradation of congo red (CR) dye under UV irradiation in an aqueous medium. In the presence of ZnO NPs photocatalytic degradation of 35% was obtained for 180 min. But Pb-ZnO, Fe-ZnO, Cd-ZnO and Pb-Fe-Cd-ZnO have shown the degradation of 45, 57, 65 and 80% respectively; they have the faster decolorization as compared with the ZnO NPs. Moreover, the photocatalyst could be reused for five times without remarkable loss of its activity.

***Keywords**: (Pb, Fe and Cd)-doped ZnO, Sonochemical method, Band gap, Photocatalytic activity.*

1. Introduction

Every day, many harmful organic pollutants are discharged into the environment from various industries. Among them, organic dyes play a vital role, owing to their great demand in textile, paper and printing industries [1]. The treatment of dye waste effluents is usually inefficient, costly and non-destructive or just transfers pollution from water to another phase. Recently, photocatalysis using semiconductor nanoparticles (TiO_2, ZnO, WO_3,) has opened a new door for the remediation of toxic organic pollutants owing to its high mineralization efficiency [2-4]. ZnO [5-7] is a very attractive semiconductor photocatalyst, for it has similar band gap energy (3.37 eV) compared with TiO_2 (3.20 eV), and its quantum efficiency is larger than that of TiO_2. There are many reports of ZnO having higher photocatalytic activities than TiO_2 in some conditions [8-13]. The main factor influencing the photocatalytic activity of ZnO is the quick recombination of charge carriers.

*Corresponding author email: m.bordbare@gmail.com
Tel.: +98 25 3210 3792; Fax: +98 25 3285 0953

In order to improve the photocatalytic activity, different kinds of ions were doped into ZnO to inhibit the recombination of photoinduced electrons and holes [10,14]. For instance, Chaudhary et al. reported Ni-doping enhanced the decolorization of dyes in ZnO [15]. Metal doping is more likely to induce the formation of vacancies or defect states which can serve as the recombination center for photogenerated electrons and holes [16].

The photocatalytic activity of transition metal doped (co-doped) semiconductors was a common feature which is higher than that of single element doped semiconductors. Wu *et al.* [17] studied the characterization of Fe and Ni co-doped ZnO nanorods synthesized using the hydrothermal method. They have reported that in the Fe-Ni co-doped ZnO the optical band gap decreases when Fe and Ni doping concentration increases [18]. Rajarajan *et al.* [1] examined the photocatalytic performance of Ni and Th co-doped ZnO nanoparticles for the degradation of methylene blue dye and showed that Ni-Th-ZnO possesses excellent photocatalytic activity for the degradation of MB when compared to that of Ni-ZnO,

Th-ZnO, ZnO and TiO_2. Zhang *et al.* [17] showed that the Er-Al co-doped ZnO exhibited enhanced photocatalytic activity and absorption ability in removing MO under visible light irradiation. Bu [19] reported that the La-Zr co-doped ZnO showed an efficient photocatalyst in photodegradation of methyl blue compared with La-doped and Zr-doped ZnO, resulting from the La and Zr synergistic effect. Karunakaran *et al.* [20] reported that doping ZnO with Cd and the hydrothermal method enhances the photocatalytic and bactericidal activities. Zhang *et al.* [21] found that Cd-doped ZnO photocatalyst had better performance than the pure ZnO; this may be due to the completely empty stable electronic configuration (d^{10}) of Cd^{2+} which shallowly traps the charge carriers and releases the same to surface adsorbed species thereby accelerating the interfacial charge transfer process. Yousaf *et al.* [22] presented that the degradation of MB, an organic dye, was increased when Fe-doped ZnO was used as a photocatalyst instead of ZnO. The trend could be attributed to the increased lifetime of exited carriers resulting from reduced bandgap by Fe incorporation. Xiao *et al.* [23] showed doping Fe into ZnO lattice introduced lots of defects, dislocations and distortions, resulting in an increased absorption of light and a decreased recombination rate of electron-hole pairs. Fe doped ZnO nanorod arrays exhibit better photocatalytic activity than that of ZnO nanocrystalline in the degradation of methyl orange (MO).

Yousefi et al. [24] revealed that the band gap of ZnO NPs was decreased when Pb concentration increased, compared to the undoped ZnO NPs. In addition, the PL results indicated more oxygen vacancies in the Pb-doped ZnO NPs than those in undoped ZnO NPs. The photocatalyst activity revealed a moderate MB removal efficiency for the Pb-doped ZnO NPs in comparison to the undoped ZnO NPs.

These previous works [18, 20-22] have demonstrated doping of Fe, Pb or Cd caused the formation of defects, dislocations, distortions and oxygen vacancies in ZnO lattice resulting in a decreasing recombination rate of electron–hole pairs. But they didn't study the photocatalytic activity of (Pb, Fe and Cd) doped ZnO. It is expected that simultaneous doping with Pb, Fe and Cd can reduce electron-hole recombination rate, resulting in the increase of photocatalytic activity.

In this paper, we described a simple sonochemical synthesis of ZnO, lead doped ZnO (Pb-ZnO), iron doped ZnO (Fe-ZnO), cadmium doped ZnO (Cd-ZnO) and (iron, lead and cadmium) doped ZnO (Pb-Fe-Cd-ZnO) nanoparticles, starting from aqueous zinc acetate as the source of zinc, and aqueous solution of NaOH as the source of oxygen without using any capping molecule. Furthermore, the effect of simultaneous doping of Pb, Fe and Cd, on the structure, optical and photocatalytic activity properties of ZnO has been studied in detail.

2. **Experimental**

2.1. Materials and equipment

All of materials used were purchased from Merck Chemical Company. The sample structures were characterized by XRD patterns obtained on a Philips model X'PertPro X-ray diffractometer using Cu Kα radiation (λ = 1.54 Å), while the morphologies of the synthetic samples were investigated by field emission scanning electron microscopy (FESEM; TESCAN-MIRA3) equipped with an Oxford Inca Energy Dispersive X-ray detector. The optical absorptions of the samples were obtained using a Shimadzu UV-2500 spectrophotometer equipped with quartz cell of 1 cm path length. Fourier transform infrared spectra (FTIR) of the samples were recorded using a Jasco model 4200 FTIR spectrophotometer over the frequency range of 400-4000 cm^{-1} using KBr as the diluent.

2.2. Sample preparation

Pb-ZnO, Fe-ZnO, Cd-ZnO, Pb-Fe-Cd-ZnO and undoped ZnO nanoparticles were synthesized by a simple sonochemical method using a sonochemical bath. To synthesize undoped ZnO, firstly 25 mL of a 0.1 M aqueous solution of zinc acetate ($Zn(Ac)_2.2H_2O$) was poured in a beaker on an ice bath and kept in a sonication bath (28 KHz, 340 W). Then, 100 mL of a 0.1 M aqueous solution of sodium hydroxide was added to this solution dropwise for about 45-50 min. Finally, the white precipitate was filtered then washed with distilled water and dried in an oven at 60 ºC for 1 h. In the presence of ultrasound following reaction occurs:

$$Zn^{2+} + 4OH^- \longleftrightarrow [Zn(OH)_4]^{2-}$$

$$2\,[Zn(OH)_4]^{2-} \xleftrightarrow{)))} 2ZnO + 4H_2 + 3O_2$$

All the steps in the synthesis of Pb-ZnO, Fe-ZnO, Cd-ZnO and Pb-Fe-Cd-ZnO NPs were similar to those of ZnO NPs, but 0.0125 mmol of lead acetate ([Pb]/[Zn]% = 0.50) for the Pb-ZnO, 0.0125 mmol of iron acetate ([Pb]/[Zn]% = 0.50) for the Fe-ZnO, 0.0125 mmol of cadmium acetate ([Cd]/[Zn]% = 0.50) for the Cd-ZnO and similar amounts of Pb, Fe and Cd for the Pb-Fe-Cd-ZnO sample were added to aqueous zinc acetate solution in the first step.

2.3. Photocatalysis conditions

In order to evaluate the photocatalytic activity of the samples, Congo red (CR) has been used as a model dye to check its degradation. The degradation with

synthesized photocatalysts was performed in a glass tube in which 0.01 g of photocatalyst powder was suspended in 25 ml of CR solution (5 mgL^{-1}). A 50 W low-pressure Hg lamp was used as a light source.

Before irradiation, the suspended solution was sonicated to disperse the catalyst in dye solution and was kept in dark for 24 h to eliminate the absorptive effect of the solution in the catalyst. While conducting experiments, the solution was continuously stirred. After irradiating the sample at a given reaction time, the catalyst was separated from dye solution. Absorbance rate of the dye solution was determined using a UV-Vis spectrophotometer and the degradation rate was evaluated by well-known degradation rate equation (Eq. 1):

$$\text{Degradation rate (\%)} = (A_0 - A)/A_0 \quad (\mathbf{1})$$

where A_0 and A are the initial absorbance and variable absorbance respectively.

3. Results and Discussion

3.1. Optical characteristics of Sample

The UV-Vis spectra of ZnO, Pb-ZnO, Fe-ZnO, Cd-ZnO and Pb-Fe-Cd-ZnO are shown in Fig. 1. It can be clearly seen that all of synthesized samples exhibit a single and well-defined absorption band at around 360 nm; this is attributed to wurtzite hexagonal structure of ZnO. The absorption edges of doped ZnO are slightly red shifted when compared to that of ZnO. The observed shift is attributed to the doping of Pb, Fe and Cd in ZnO. The optical band gaps are determined using Tauc equation [25,26] (Eq. 2):

$$(\alpha h\nu)^2 = C\,(h\nu - E_g) \quad (\mathbf{2})$$

Where α is the absorption coefficient, C is a constant, hν is the photon energy and E_g is the band gap. Tauc plots of ZnO, Pb-ZnO, Fe-ZnO, Cd-ZnO and Pb-Fe-Cd-ZnO are given in Fig. 1. The optical band gaps are found to be 3.18 eV, 3.14 eV, 3.12, 3.05 and 3.00 eV for ZnO, Pb-ZnO, Fe-ZnO, Cd-ZnO and Pb-Fe-Cd-ZnO, respectively (Table 1);these results are due to the excess carriers provided by Cd, Fe and Pb doping can fill some energy levels on the edge of conduction band and cause the transition energy decrease [10,11]. Thus, the metal doped ZnO could exhibit a higher photocatalytic activity than bare ZnO.

3.2. Structural characteristics

The XRD patterns of doped ZnO and undoped ZnO NPs are shown in Fig. 2. For all samples of ZnO NPs, all five visible diffraction peaks are indexed to wurtzite structure ZnO (JCPDS Card No. 80-0075), and no additional peak attributed to Pb, Fe and Cd or their oxide is detected in our samples.

The ionic radius of the substitutes Pb^{2+} (R^{2+}=1.19 Å) and Cd^{2+} (R^{2+}=0.95 Å) are bigger than that of Zn^{2+} (R^{2+}=0.74 Å). But the ionic radius of the Fe^{2+} (R^{2+}=0.61 Å) is smaller than that of Zn^{2+} (R^{2+}=0.74 Å).

Thus, doping with Pb and Cd caused a slight shift in the XRD Peaks toward lower diffraction angles and doping with Fe caused positive shift. This result provides indirect evidence that Pb^{2+}, Fe^{2+} and Cd^{2+} incorporated into the crystal structure, caused the ZnO crystal lattice to expand. Substitution of Zn by a larger atom would cause an increase in the c-lattice constant, which reflects as the peak shift to lower angle on XRD pattern and vice versa [23]. The crystalline size of the ZnO NPs was determined by means of an X-ray line-broadening method, using the Scherrer equation (Eq. 3):

$$D = k\lambda/\beta\cos\theta \quad (\mathbf{3})$$

Where D is the crystalline size, b is the full width half maximum (FWHM) of the 2θ peak, K is the shape of particle factors (it equals to 0.89), θ and l are the incident of angle and wavelength of the X-rays, respectively. The (101) plane was chosen to calculate the crystalline size (either plane can be used for this purpose). The crystalline size of ZnO, Pb-ZnO, Fe-ZnO, Cd-ZnO and Pb-Fe-Cd-ZnO NPs was estimated about 26.45, 22.04, 22.79, 24.97 and 16.50 nm respectively (Table 1). The results revealed that there are a reduction in the crystalline size of ZnO after doping with Pb, Fe and Cd.

The FE-SEM images of the undoped and doped ZnO NPs are shown in Fig. 3. Nearly spherical shapes with particle sizes distributed over the nanometer range can be seen and samples with Pb, Fe and cd doped ZnO have non-spherical shapes. The composition of doped ZnO and undoped ZnO was determined by the elemental dispersion analysis using X-ray (EDS) measurements. The EDS results confirm the presence of the elements zinc, lead, iron, cadmium and oxygen. Typical EDS of Pb-Fe-Cd-ZnO are shown in Fig. 4.

The characterizations of functional groups of undoped and doped samples were investigated using Fourier transform infrared (FT-IR) spectroscopy at room temperature in the range of 400-4000 cm^{-1} and the results are shown in Fig. 5. FT-IRs of the ZnO and doped ZnO NPs (Fig. 5) show strong peaks at 560 cm^{-1} to 460 cm^{-1} indicating the formation of Zn-O [9]. Moreover, in undoped and doped samples, no obvious changes can be seen in FTIR spectra. It is worth mentioning that Pb, Fe and Cd atoms were successfully incorporated into the crystal lattice of ZnO. Therefore, it is reasonable to conclude that synthetic product has no significant impurity [27]. Absorption bands near 1600 cm^{-1} and 3411 cm^{-1} represent O-H stretching and bending mode of vibrations of water respectively.

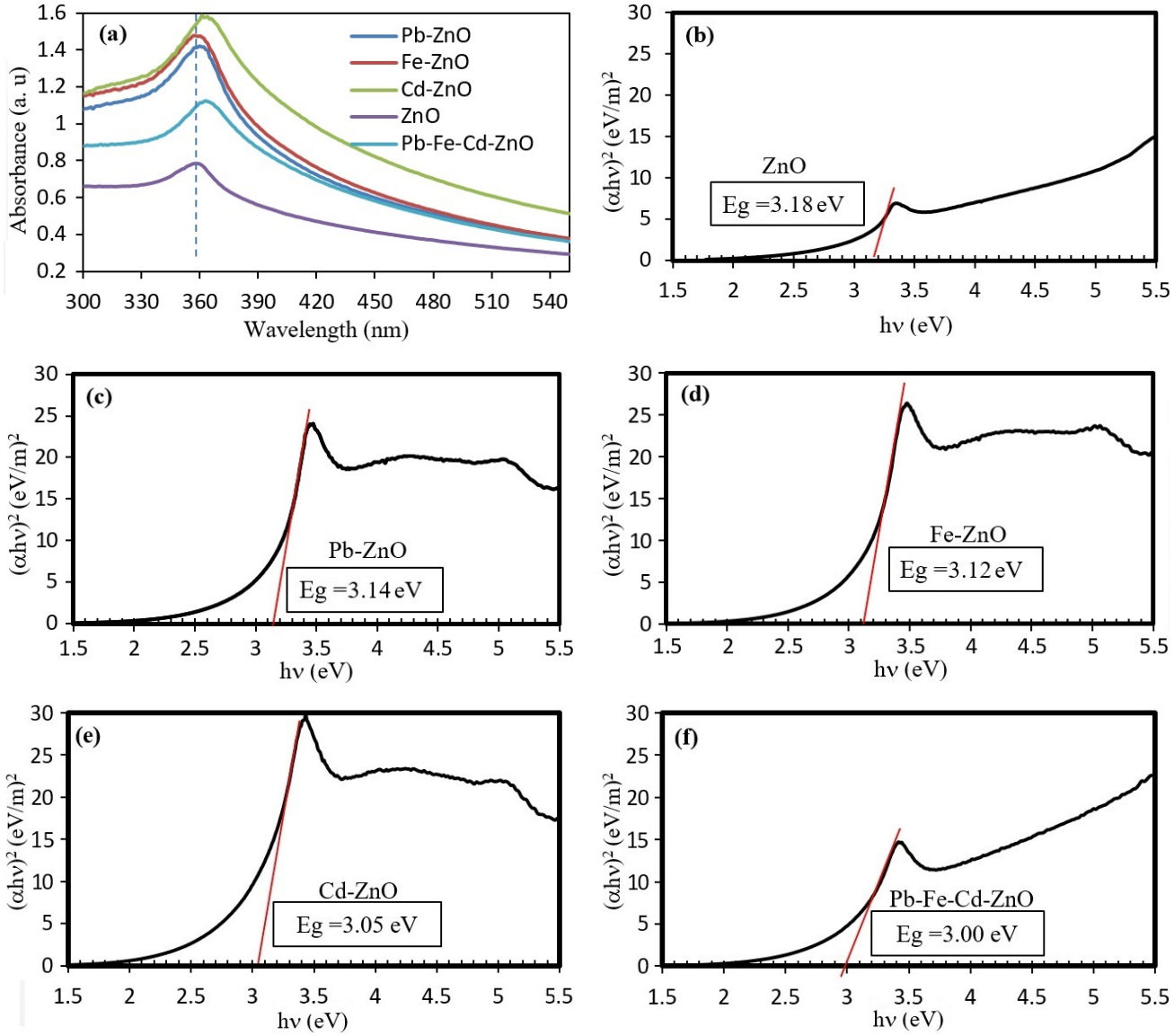

Fig. 1. (a) UV-Vis absorption spectra of samples and (b-f) plots of $(\alpha h\nu)^2$ as a function of photon energy ($h\nu$) for the undoped ZnO and doped ZnO.

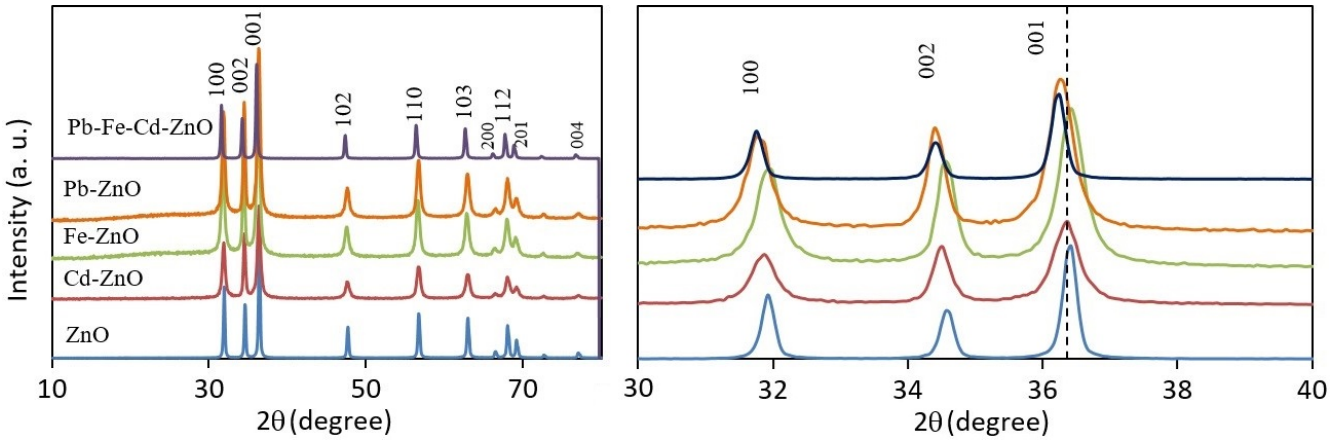

Fig. 2. XRD patterns for (a) undoped and doped ZnO NPs, (b) expanded view between 2θ=30-40°.

Table 1. Peak position, band gap, crystal size of samples and %degradation of CR in the presence of synthesized photocatalysts.

Samples	Crystal Size (nm)	Wavelength (nm)	Bandgap (eV)	Degradation (%)
ZnO	26.45	358	3.18	35
Pb-ZnO	22.04	359	3.14	45
Fe-ZnO	22.79	360	3.12	57
Cd-ZnO	24.97	361.5	3.05	65
Pb-Fe-Cd-ZnO	16.50	363	3.00	80

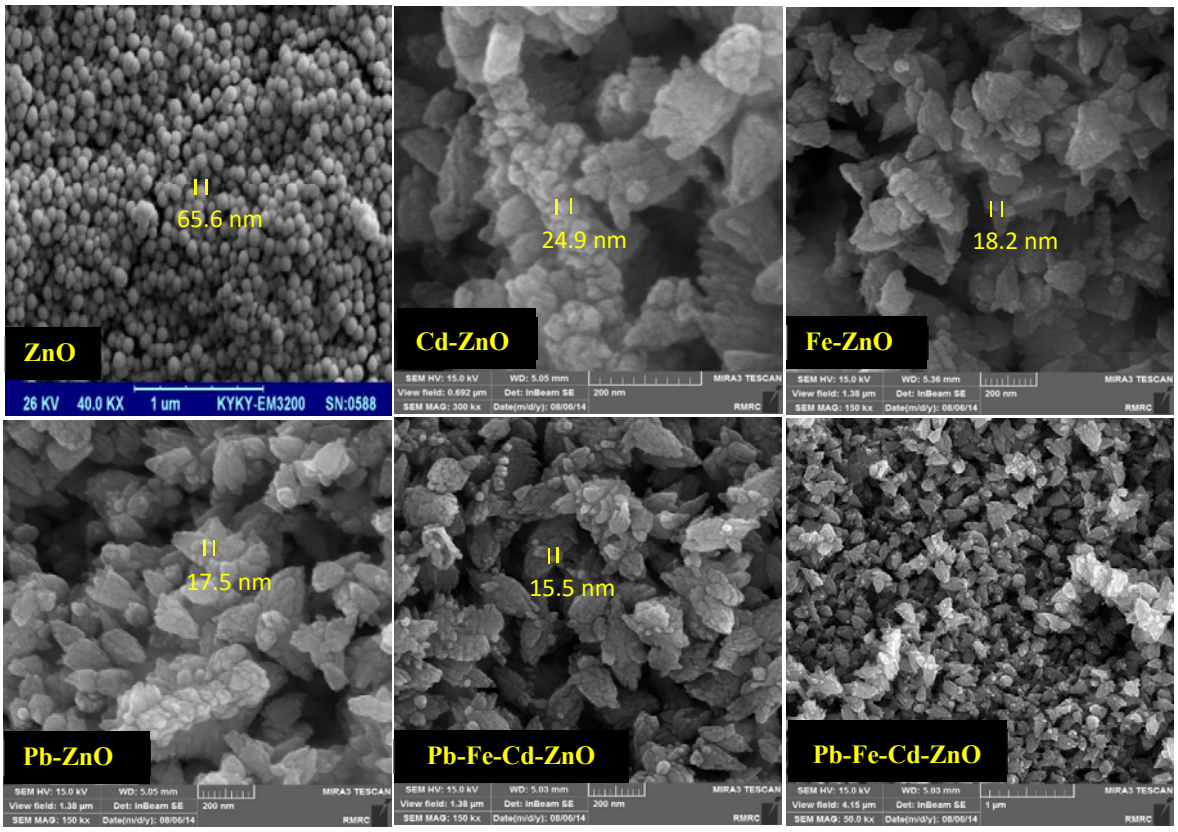

Fig. 3. SEM image of ZnO and FE-SEM images of doped ZnO NPs prepared by sonochemical method.

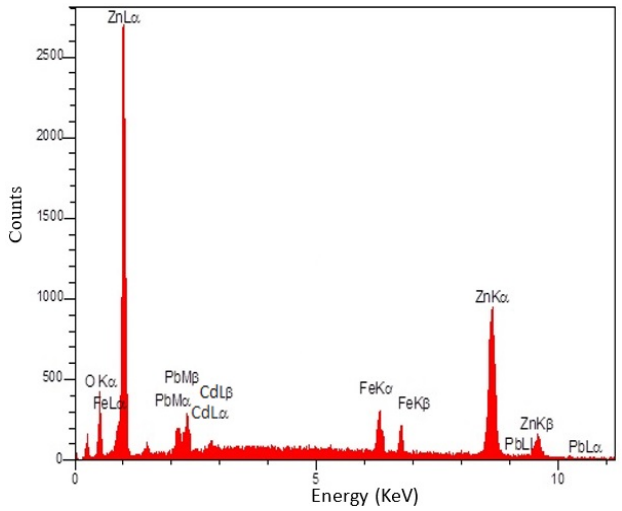

Fig. 4. EDS pattern obtained for the Pb-Fe-Cd-ZnO.

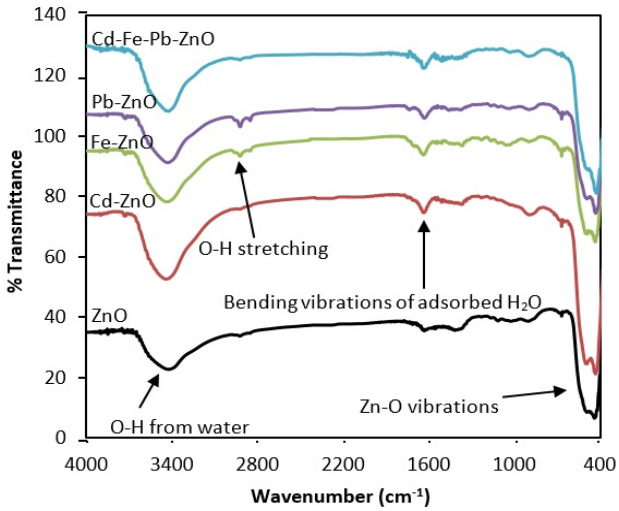

Fig. 5. FTIR spectra of ZnO and doped ZnO NPs.

3.3. Photocatalytic activity

The photocatalytic activity of the ZnO and doped ZnO NPs was carried out under UV irradiation and tested using the UV-Vis spectrophotometer. In the presence of Pb-Fe-Cd-ZnO photocatalyst, absorption maximum (in the λ=500 nm) of CR gradually decreased upon exposure to UV light irradiation shown in Fig. 6a. This shows that the degradation and decolorization of aqueous CR were strictly due to the catalyst activity under UV irradiation. The effect of degradation was calculated using the ratio between the C_0 (absorption maximum at time, t = 0) and C_t (absorption maximum at certain degradation time). The photocatalytic degradation of CR in the presence of ZnO and different doped ZnO NPs as catalysts is shown in Fig. 6b. From the figure, it is clear that in the presence of ZnO NPs photocatalytic degradation of 35% was obtained but the degradations of 45, 57, 65 and 80% were obtained using Pb-ZnO, Fe-ZnO, Cd-ZnO and Pb-Fe-Cd-ZnO in 180 min., which have the faster decolorization as compared with the ZnO NPs [28].

The kinetic data of the photocatalytic degradation of CR using ZnO and doped ZnO samples fit well to the apparent first-order reaction kinetics as shown in Fig. 6b. The apparent first-order reaction rate constant (k) was calculated by the slopes of these curves for pure and doped ZnO [29]. It is observed that degradation of CR in the presence Pb-Fe-Cd-ZnO photocatalyst has highest k.

A simple mechanism to understand the enhancement of photocatalytic activity of doped ZnO photocatalysts is shown in Fig. 7. When the NPs are irradiated with UV light, electrons in the valence band (VB) are transferred to the conduction band (CB) ($O_{2p} \rightarrow Zn_{3d}$), leading to the formation of the same number of holes in the VB and initiating a series of reactions to produce hydroperoxyl radicals ($HO_2\cdot$) and hydroxyl radicals ($OH\cdot$). These hydroxyl radicals are strong oxidants that can decompose organic pollutants [24]. In the process, undesirable recombination of electrons and holes may also rapidly occur, reducing the photocatalytic activity. The Pb^{2+}, Fe^{2+} and Cd^{2+} dopants may accept the electrons in the CB of ZnO to form Pb^{+}, Fe^{+} and Cd^{+}. Then the as-formed Pb^{+}, Fe^{+} and Cd^{+} may transport an electron to the dissolved O_2 to produce superoxide radical anions, thereby inhibiting the recombination of photo-induced electrons and holes.

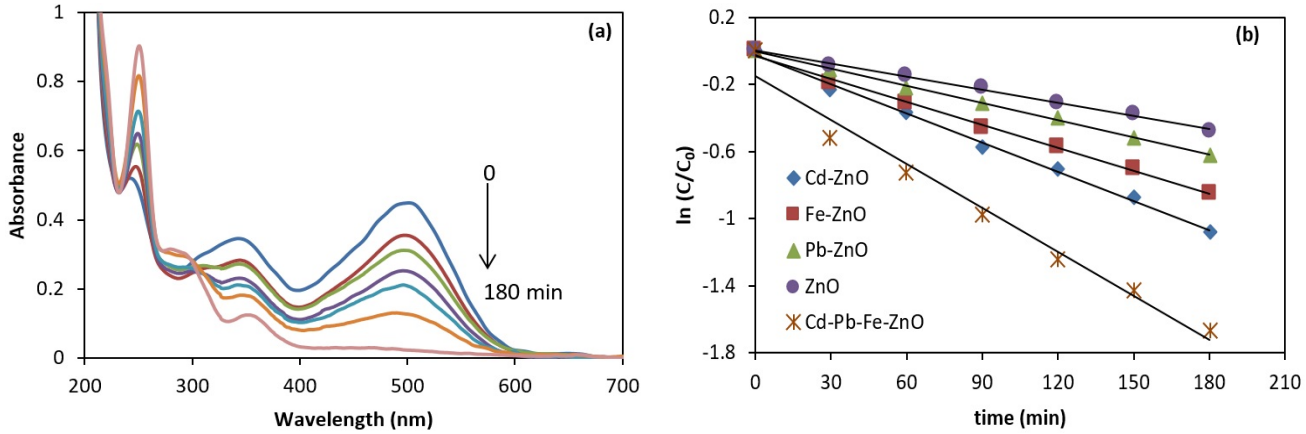

Fig. 6. (a) UV-Vis spectra of the aqueous solutions of CR dye after UV irradiation for different time periods (0-180 min) in the presence of Pb-Fe-Cd-ZnO NPs photocatalyst (0.4 gL^{-1}), (b) Typical ln(C/C_0) versus irradiation time plots using ZnO and doped ZnO NPs (0.4 gL^{-1}).

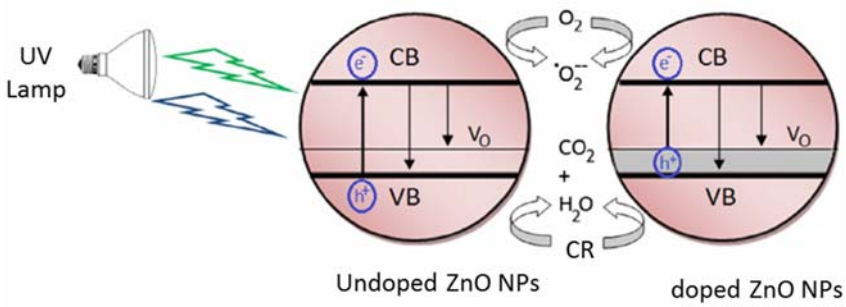

Fig. 7. Schematic representation of the photocatalytic mechanism for the undoped and doped ZnO NPs under UV light [24].

This means that Pb^{2+}, Fe^{2+} and Cd^{2+} on the surface of the ZnO NPs may act as an electron scavenger [24]. The enhancement of the multi-element doping on the photocatalytic activity of ZnO has not been well understood. According to the fact that doping with Pb^{2+}, Fe^{2+} and Cd^{2+} alone has a little effect on the photocatalytic, we think that there might exist a cooperative enhancement on the activity in the multi-element doping system. The presence of cadmium, iron and lead traps the electron from the CB of ZnO, and simultaneously suppresses the photo-excited electron-hole recombination. This enhances the photocatalytic activity of Pb-Fe-Cd-ZnO due to a synergistic effect among Pb, Fe and Cd [19].

3.4. Reusability of Pb-Fe-Cd-ZnO

Obviously, recoverability and reusability are the advantages of heterogeneous catalysts, especially for commercial and industrial applications. The recyclability test of the Pb-Fe-Cd-ZnO photocatalyst was also carried out. The Pb-Fe-Cd-ZnO photocatalyst can be easily separated from the reaction mixture by brief centrifugation and multiple washings with distilled water followed by drying. The recovered photocatalyst was evaluated in the degradation of CR. Pb-Fe-Cd-ZnO was recycled five times to obtain 71% degradation of CR, as monitored by UV-Vis spectroscopy (Fig. 8). The catalytic activity did not decrease considerably after five catalytic cycles. This demonstrates the high stability and catalytic activity of the catalyst under operating conditions.

4. Conclusions

Pb-ZnO, Fe-ZnO, Cd-ZnO and Pb-Fe-Cd-ZnO NPs were successfully synthesized through a facile one-pot sonochemical method. XRD results revealed that all synthesized samples showed a hexagonal wurtzite ZnO structure. Also, Cd, Fe and Pb ions were successfully doped in to ZnO. UV-Vis absorption spectra showed a red shift in doped sample compared to ZnO. The observed red shift of energy gap is explained by sp–d exchange interactions between the band electrons and the localized d-electrons of the Pb^{2+}, Fe^{2+} and Cd^{2}ions. Moreover, the photocatalytic activity in the degradation of various dyes in water has also been investigated. The Pb-Fe-Cd-ZnO showed an efficient photocatalyst in photodegradation of CR compared with Pb-ZnO, Fe-ZnO and Cd-ZnO following the Cd, Fe and Pb synergistic effect. Furthermore, the photocatalyst can be recovered and recycled five times without significant loss of catalytic activity in this methodology, making this procedure environmentally more acceptable.

Acknowledgements

We gratefully acknowledge the Payame Noor University for the Support of this work.

References

[1] K. Vignesh, M. Rajarajan, A. Suganthi, J. Ind. Eng. Chem. 20 (2014) 3826-3833.
[2] K. Vignesh, R. Priyanka, M. Rajarajan, A. Suganthi, Mater. Sci. Eng. B 178 (2013) 149-157.
[3] Y. Shavisi, S. Sharifnia, S.N. Hosseini, M.A. Khadivi, J. Ind. Eng. Chem. 20 (2014) 278-283.
[4] K. Vignesh, R. Hariharan, M. Rajarajan, A. Suganthi, Solid State Sci. 21 (2013) 91-99.
[5] L. Vafayi, S. Gharibe, Iran. J. Catal. 5 (2015) 365-371.
[6] M. Bordbar, S. Forghani-pilerood, A. Yeganeh-Faal, Iran. J. Catal. 6 (2016) 415-421.
[7] S. Aghdasi, M. Shokri, Iran. J. Catal. 6 (2016) 481-487.
[8] M. Bordbar, B. Khodadadi, N. Mollatayefe, A. Yeganeh-Faal, J. Appl. Chem. 8 (2013) 43-48.
[9] M. Bordbar, S.M. Vasegh, S. Jafari, A.Y. Faal, Iran. J. Catal. 5 (2015) 135-141.
[10] M. Bordbar, A. Yeganeh-Faal, B. Khodadadi, J. Nanostruct. 6 (2016) 190-198.
[11] B. Khodadadi, M. Bordbar, Iran. J. Catal. 6 (2016) 37-42.

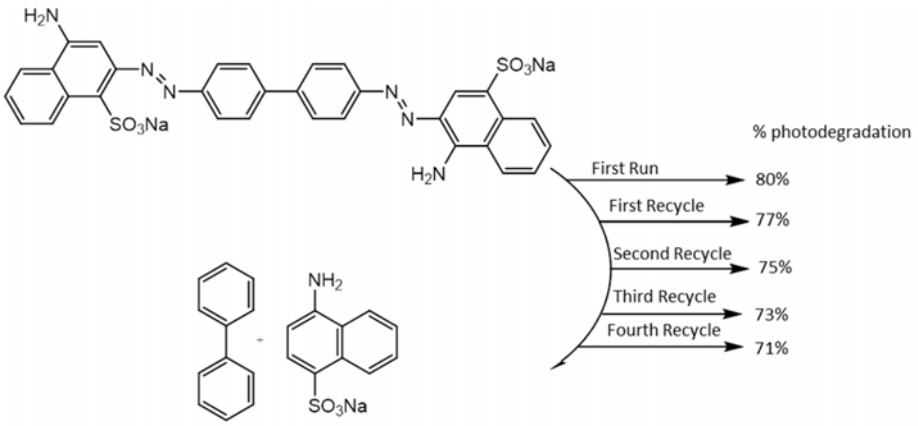

Fig. 8. Reusability of the Pb-Fe-Cd-ZnO photocatalyst (0.01 g) in Photodegradation of 25 mL CR (5 mgL^{-1}).

[12] B. Khodadadi, M. Bordbar, M. Sajedi, J. Appl. Chem. Res. 8 (2014) 35-44.
[13] B. Khodadadi, M. Bordbar, A. Yeganeh-Faal, J. Sol-Gel Sci. Technol. 77 (2016) 521-527.
[14] J. Zhao, L. Wang, X. Yan, Y. Yang, Y. Lei, J. Zhou, Y. Huang, Y. Gu, Y. Zhang, Mater. Res. Bull. 46 (2011) 1207-1210.
[15] P. Saharan, G.R. Chaudhary, S. Lata, S. Mehta, S. Mor, Ultrason. Sonochem. 22 (2015) 317-325.
[16] W. Yu, J. Zhang, T. Peng, Appl. Catal. B 181 (2016) 220-227.
[17] X. Zhang, S. Dong, X. Zhou, L. Yan, G. Chen, S. Dong, D. Zhou, Mater. Lett. 143 (2015) 312-314.
[18] X. Wu, Z. Wei, L. Zhang, C. Zhang, H. Yang, J. Jiang, Ceram. Int. 40 (2014) 14635-14640.
[19] H.F. Moafi, M.A. Zanjanch, A.F. Shojaie, J. Nanosci. Nanotechnol. 14 (2014) 7139-7150.
[20] C. Karunakaran, A. Vijayabalan, G. Manikandan, Superlattices Microstruct. 51 (2012) 443-453.
[21] D. Zhang, F. Zeng, J. Mater. Sci. 47 (2012) 2155-2161.
[22] M. Yousaf, H. Rafique, M. Amin, S. Ramay, S. Atiq, N. Alzayed, S. Siddiqi, Dig. J. Nanomater. Biostruct. 12 (2017).
[23] S. Xiao, L. Zhao, J. Lian, Catal. Lett. 144 (2014) 347-354.
[24] R. Yousefi, F. Jamali-Sheini, M. Cheraghizade, L. Zaman, Mater. Res. Innovations 20 (2016) 121-127.
[25] J. Tauc, R. Grigorovici, A. Vancu, Phys. Status Solidi 15 (1966) 627-637.
[26] S. Jafari, A. Nezamzadeh-Ejhieh, J. Colloid Interface Sci. 490 (2017) 478-487.
[27] C.K. Ghosh, S. Malkhandi, M.K. Mitra, K.K. Chattopadhyay, J. Phys. D: Appl. Phys. 41 (2008) 245113-245113.
[28] K. Ranjith, B. Kiruthika, R. Rajendrakumar, J. Microsc. 252 (2013) 217-225.
[29] A. Nezamzadeh-Ejhieh, Z. Banan, Iran. J. Catal. 2 (2012) 79-83.